

# Lyapunov-Based Controller Synthesis and Stability Analysis for the Execution of High-Speed Multi-Flip Quadrotor Maneuvers

Ying Chen and Néstor O. Pérez-Arancibia

**Abstract**— We present a method for the synthesis and stability analysis of automatic controllers capable of autonomously flying a 19-gram quadrotor during the execution of high-speed multi-flip maneuvers. The discussed approach for design and analysis is based on Lyapunov’s direct method, numerical results and experimental data. Here, the resulting real-time closed-loop scheme employs a *linear time-invariant* (LTI) controller that stabilizes the nonlinear unstable dynamics of the open-loop system while enabling high performance during aggressive flight. In this approach, we define a parameterized quadratic *proto*-Lyapunov function associated with the nonautonomous closed-loop flyer’s dynamics that, for a set of feasible parameters, becomes Lyapunov. This parameterization allows for the synthesis and selection of stabilizing controllers which are tested through numerical simulation, employing an open-loop plant model obtained from first principles and simple system identification experiments. The suitability of the proposed method is empirically demonstrated through several aggressive autonomous flight experiments that include single, double and triple flips about two different axes of the flyer.

## I. INTRODUCTION

The vision of creating fully autonomous squadrons of *unmanned micro air vehicles* (UMAVs) capable of operating in highly unstructured environments will become possible only when each individual flyer becomes proficient in the autonomous execution of sophisticated high-speed maneuvers. In [1], we presented a series of experimental results demonstrating high-speed maneuvers of a 19-gram quadrotor, achieved with the use of a switching controller composed of two *linear time-invariant* (LTI) subsystems. There, one LTI sub-controller is employed during regular autonomous flight, and the other sub-controller is used during high-speed flipping. Here, we discuss in depth the method for synthesizing the controller employed during aerobatic flight, which is constructed upon Lyapunov’s direct method for stability [2], [3].

Over the years, Lyapunov’s theory has been demonstrated to be an effective tool for nonlinear system stability analysis and feedback controller synthesis. In the case presented here, after a control structure is chosen, stabilizing controller parameters can be obtained by defining a parameterized *proto*-Lyapunov function that, when combined with the use of Lyapunov’s direct method, informs us of the stability properties of the closed-loop system dynamics. This proposed synthesis method can be extended to formulate optimization problems to obtain controllers that are not only stable, but also make the system robust with respect to model

This work was partially supported by the *National Science Foundation* (NSF) through award NRI 1528110 and the USC Viterbi School of Engineering through a graduate fellowship to Y. Chen and a start-up fund to N. O. Pérez-Arancibia. Any opinions, findings, and conclusions or recommendations expressed in this material are those of the authors and do not necessarily reflect the views of the NSF.

The authors are with the Department of Aerospace and Mechanical Engineering, University of Southern California (USC), Los Angeles, CA 90089-1453, USA (e-mail: chen061@usc.edu; perezara@usc.edu).

uncertainty and external disturbances, while simultaneously considering stability and performance. Parameterized *proto*-Lyapunov functions can also be employed to synthesize sets of simple controllers for the execution of sequenced flight maneuvers constituting the *primitives*<sup>1</sup> required for the creation of autonomous behavior. Furthermore, the proposed approach can be applied to the high-speed control of other micro flyers such as the artificial insects in [6] and [7].

Recently, a significant amount of research has been published on the dynamic modeling and control of quadrotors. In this context, numerous papers describe the use of control techniques based on Lyapunov’s stability theory [8]–[18], validated mostly through simulations or simple non-aggressive flight experiments. This technical literature includes backstepping nonlinear control [8]–[10], feedback-linearization-based control [11], adaptive sliding-mode control [11], [12], adaptive fuzzy control [13], quaternion-based *proportional-derivative* (PD) attitude control [14], nonlinear geometric control [17] and neural-networks-based control [18], to mention a few examples. The methods and ideas presented in those publications represent interesting progress on the understanding of quadrotor dynamics and control. However, due to the lack of concrete empirical evidence and compelling experimental results, their applicability is very limited and not well suited for real-life scenarios. On the other hand, advanced experimental research [19], [20] has mostly ignored the fundamental issue of closed-loop system stability from the theoretical perspective. In this paper, we contribute the first step in a long-term research program that aims to produce the experimental and theoretical tools necessary for the creation of truly autonomous flying robots that can operate in highly-unstructured time-varying noisy environments.

The rest of the paper is organized as follows. Section II discusses the nonlinear dynamics of the quadrotor. Section III presents the proposed controller structure, parameterized *proto*-Lyapunov function used for controller design, proposed controller synthesis method based on Lyapunov’s direct method, and attitude analysis. Section IV presents simulation and experimental results. Conclusions are drawn in Section V.

## Notation—

- $\mathbb{R}, \mathbb{R}^+$  denote the sets of reals and nonnegative reals.
- The symbols  $|\cdot|, \|\cdot\|_2, \|\cdot\|_2$  and  $\|\cdot\|_\infty$  denote the scalar absolute value, vector 2-norm, matrix induced 2-norm and matrix induced  $\infty$ -norm, respectively.
- Scalars are denoted by regular lower-case or upper-case letters (e.g.,  $m, \Omega_1$ ). Vectors are denoted by bold lower-case letters (e.g.,  $\omega$ ). Matrices are denoted by bold upper-case letters (e.g.,  $K_p$ ). Quaternions are denoted

<sup>1</sup>Fundamental units or blocks of action as defined in [4] and [5].

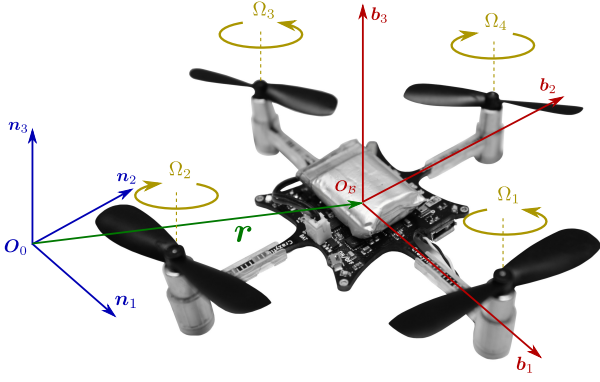


Fig. 1: **The flyer and frames of reference.**  $\mathcal{N} = \{O_0, n_1, n_2, n_3\}$  is the inertial frame,  $\mathcal{B} = \{O_B, b_1, b_2, b_3\}$  is the body frame,  $r$  indicates the position of the flyer's center of mass with respect to the inertial origin  $O_0$  and  $\{\Omega_1, \Omega_2, \Omega_3, \Omega_4\}$  are the angular speeds of the rotors. The test platform employed in the flight experiments is the Crazyflie 1.0 [21], which weighs 19 grams and has a maximum *propeller-tip-to-propeller-tip* (PTPT) distance of 13 cm. Due to symmetry, if the blade masses are neglected, the axes  $\{b_1, b_2, b_3\}$  coincide with the flyer's principal axes of inertia; therefore, the inertia matrix  $J$  when expressed in  $\mathcal{B}$  is constant and diagonal.

by crossed bold lower-case letters (e.g.,  $\mathbf{q}$ ).

- The symbol  $*$  denotes the quaternion product (e.g.,  $\mathbf{q} * \mathbf{p}$ ), as defined in [22].
- The letter  $s$  denotes the differentiation operator, and equivalently, the Laplace variable.
- The letter  $t$  denotes continuous time, and  $t_0$ , the initial time of an experiment. We assume  $t \geq 0$ .

## II. OPEN-LOOP MODEL OF THE SYSTEM

In this section, we introduce the dynamic model of the quadrotor, shown in Fig. 1, and discuss the underlying assumptions behind its conception. To represent the kinematics and dynamics of the system, we define the inertial frame  $\mathcal{N} = \{O_0, n_1, n_2, n_3\}$  and the body-fixed frame  $\mathcal{B} = \{O_B, b_1, b_2, b_3\}$ , whose origin and axes coincide with the quadrotor's center of mass and principal axes, as depicted in Fig. 1. Thrust is generated by four propellers rotating with angular speeds  $\{\Omega_1, \Omega_2, \Omega_3, \Omega_4\}$ . Using these conventions, it follows that the nonlinear dynamics of the flyer are given by

$$m\ddot{\mathbf{r}} = -mg\mathbf{n}_3 + \phi\mathbf{b}_3, \quad (1)$$

$$\mathbf{J}\dot{\boldsymbol{\omega}} = -\boldsymbol{\omega} \times \mathbf{J}\boldsymbol{\omega} + \boldsymbol{\tau}, \quad (2)$$

where  $m$  is the total mass of the flyer;  $\mathbf{r}$ ,  $\dot{\mathbf{r}}$  and  $\ddot{\mathbf{r}}$  are the spatial position, velocity and acceleration of the flyer's center of mass with respect to, and expressed in,  $\mathcal{N}$ ;  $g$  is the gravitational acceleration constant;  $\phi = \sum_{i=1}^4 \phi_i$  is the magnitude of the total thrust force produced by the four propellers, where  $\phi_i$  denotes the magnitude of the thrust force produced by the  $i$ th propeller;  $\mathbf{J}$  is the robot's inertia matrix, which by neglecting the blade masses is assumed constant and diagonal when expressed in  $\mathcal{B}$ ;  $\boldsymbol{\omega}$  is the quadrotor's angular velocity with respect to  $\mathcal{N}$  with its components expressed in  $\mathcal{B}$ ; and  $\boldsymbol{\tau} = [\tau_1 \ \tau_2 \ \tau_3]^T$  is the total torque applied by the rotors to the vehicle with its components expressed in  $\mathcal{B}$ .

As discussed in [1],  $\boldsymbol{\tau}$  and  $\phi$  depend directly on the propeller's angular speeds  $\{\Omega_1, \Omega_2, \Omega_3, \Omega_4\}$  through the relationship

$$\boldsymbol{\vartheta} = \boldsymbol{\Gamma}\boldsymbol{\vartheta}, \quad (3)$$

where  $\boldsymbol{\vartheta} = [\phi \ \boldsymbol{\tau}^T]^T$ ,  $\boldsymbol{\vartheta} = [\Omega_1^2 \ \Omega_2^2 \ \Omega_3^2 \ \Omega_4^2]^T$ , and  $\boldsymbol{\Gamma}$  is a  $4 \times 4$  real matrix that depends on the quadrotor's geometry and experimentally identifiable parameters. See [1] for further details on the structure of  $\boldsymbol{\Gamma}$ . In the obtention of the model described by (1) and (2), we ignore motor latency, gyroscopic effects and aerodynamic effects produced by the flyer's translational motion. Also, by ignoring the blade-flapping effect, the direction of the total thrust force,  $\phi$ , is assumed to be perpendicular to the  $b_1$ - $b_2$  plane and aligned with the  $b_3$  axis. These simplifications allow for the derivation of a nominal plant that reduces the complexity of the dynamical analysis while facilitating the controller design process. A complete model of the system, including disturbances, will be discussed in a future publication.

Using the notion of quaternions as defined in [22], the attitude kinematics of the flyer can be described as

$$\dot{\mathbf{q}} = \frac{1}{2}\mathbf{Q}(\mathbf{q})\boldsymbol{\omega}, \quad (4)$$

where  $\mathbf{q} = [q_0 \ q_1 \ q_2 \ q_3]^T$  and

$$\mathbf{Q}(\mathbf{q}) = \begin{bmatrix} -q_1 & -q_2 & -q_3 \\ q_0 & -q_3 & q_2 \\ q_3 & q_0 & -q_1 \\ -q_2 & q_1 & q_0 \end{bmatrix}. \quad (5)$$

This allows us to represent the entire dynamical system in the standard state-space form as

$$\dot{\boldsymbol{\chi}} = \boldsymbol{\psi}(\boldsymbol{\chi}, \boldsymbol{\vartheta}), \quad (6)$$

where  $\boldsymbol{\chi} = [\mathbf{r}^T \ \dot{\mathbf{r}}^T \ \mathbf{q}^T \ \boldsymbol{\omega}^T]^T$  and  $\boldsymbol{\vartheta}$  is given by (3). Note that there are several implicit algebraic and physical facts in the structure of (6), and its constituent sub-states, that are important to emphasize. In (1),  $b_3$  depends on  $\mathbf{q}$ , and in (2),  $\boldsymbol{\tau}$  is strongly coupled with  $\{\phi_1 \ \phi_2 \ \phi_3 \ \phi_4\}$ . Also, the part of the state-space model in (6) associated with  $\boldsymbol{\omega}$  is independent of the rest of the system, and  $\dot{\boldsymbol{\omega}} = \mathbf{J}^{-1}(\boldsymbol{\tau} - \boldsymbol{\omega} \times \mathbf{J}\boldsymbol{\omega})$  therefore evolves independently. Thus,  $\boldsymbol{\omega}$  can be seen as an external input driving the angular position dynamics in (4), and since  $b_3$  depends on  $\mathbf{q}$ ,  $\mathbf{q}$  acts as an external input driving the translational dynamics in (1). The characteristics of (6) are key pieces of information used in the formulation of the controller design method and stability analysis discussed in the next section.

During the execution of a multi-flip maneuver, the quadrotor rises with a predefined initial upward speed and then drops freely until the body rotation is completed, tracking a desired angular velocity trajectory. In this process, the direction of the thrust force changes quickly and periodically, exerting no significant effect on the translational motion of the flyer. Thus, gravity is assumed to be the only external force applied to the flyer while multi-flipping at high speeds. For this reason, in the proposed control scheme, the translational dynamics of the flyer are kept in open-loop, and the control problem of rotational motion is formulated independently of the rest of the state. The multi-flip process is explained in detail in [1].

## III. CONTROL STRUCTURE, CONTROLLER SYNTHESIS, STABILITY ANALYSIS, AND NOMINAL PERFORMANCE

### A. Angular Velocity Dynamics and Closed-Loop Control

Considering the open-loop independence of (2) with respect to the rest of the state-space system in (6), we propose a control strategy based on the feedback stabilization of

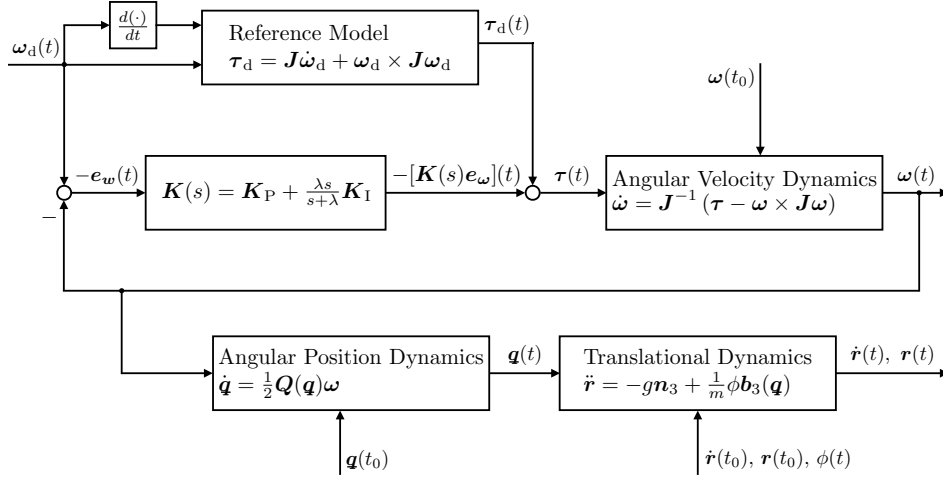


Fig. 2: **Dynamics of the robot and feedback control scheme.** The nonlinear dynamics associated with the flyer’s angular velocity are controlled employing a reference model that computes a feasible desired torque  $\tau_d$  given a reference angular velocity  $\omega_d$ . Concurrently, deviations from the desired trajectory  $\omega_d$  are compensated with a stabilizing feedback LTI MIMO controller with the form  $K(s) = K_P + \frac{\lambda s}{s+\lambda} K_I$ . The parameters in the entries of constant diagonal matrices  $K_P$  and  $K_I$  are chosen so that the parameterized *proto*-Lyapunov function  $\mu(\mathbf{x})$  becomes Lyapunov and the closed-loop system is stable. In the analysis and controller synthesis process, a perfect matching between the reference model and *true* system dynamics is assumed. Also, it is assumed that the system is not subjected to external disturbances. Since model uncertainty and the effect of disturbances are ignored in the design process, only nominal stability is guaranteed from the theoretical perspective; performance and stability robustness are tuned and tested experimentally. Note that the angular position and translational dynamics remain in open loop. Using quaternion theory, we explicitly show the nominal BIBO stability of the first open-loop system. The second open-loop system is not stable and slow translational drift is expected. This slow drift is not significant during the execution of multi-flip maneuvers because they are completed in less than 2 s.

(2), while achieving high performance in the tracking of a physically feasible reference  $\omega_d$ . This objective is achieved with the control scheme in Fig. 2, where the control signal is generated according to the law

$$\tau = -\left[ K_P + \frac{\lambda s}{s+\lambda} K_I \right] e_\omega + \tau_d, \quad (7)$$

where  $\tau_d$  is the desired torque to be applied to the flyer, and  $e_\omega = \omega - \omega_d$  is the control error between the measured angular velocity,  $\omega$ , and desired angular velocity,  $\omega_d$ . The components of  $e_\omega$ , expressed in  $\mathcal{B}$ , are denoted by  $\{e_{\omega_1}, e_{\omega_2}, e_{\omega_3}\}$ . In this scheme, shown in Fig. 2, the *multiple-input–multiple-output* (MIMO) controller  $K(s)$  is determined by the constant scalar  $\lambda$ , and the constant diagonal matrices  $K_P$  and  $K_I$ , whose parameters are computed using the proposed Lyapunov-based method described below.

To begin the parameterization process for analysis and controller design, we rewrite the angular velocity dynamics in (2) as

$$J\dot{\omega} + \mathbf{f}(\omega) = \tau, \quad (8)$$

with

$$\mathbf{f}(\omega) = \omega \times J\omega = \begin{bmatrix} (j_{33} - j_{22})\omega_2\omega_3 \\ (j_{11} - j_{33})\omega_1\omega_3 \\ (j_{22} - j_{11})\omega_1\omega_2 \end{bmatrix} = \begin{bmatrix} f_1(\omega) \\ f_2(\omega) \\ f_3(\omega) \end{bmatrix}, \quad (9)$$

where  $\{j_{11}, j_{22}, j_{33}\}$  are the diagonal entries of  $J$  and  $\{\omega_1, \omega_2, \omega_3\}$  are the components of  $\omega$ , expressed in  $\mathcal{B}$ . Similarly, the reference model used in the control scheme of Fig. 2 can be rewritten as

$$J\dot{\omega}_d + \mathbf{f}(\omega_d) = \tau_d, \quad (10)$$

where  $\omega_d$  is the time-dependent signal to be tracked in order to perform a desired multi-flip aerobatic maneuver. For practical and analytical reasons,  $\omega_d$  is chosen to be bounded, Lipschitz continuous and complying with the system’s physical limitations. In addition,  $\omega_d$  is chosen so that the function

$\mathbf{f}$  remains differentiable along the reference trajectory  $\omega_d$ . With these definitions in mind and recalling the standard linearization technique along a feasible system trajectory, we can write

$$\mathbf{f}(\omega) = \mathbf{f}(\omega_d) + \mathbf{A}_f(\omega_d)(\omega - \omega_d) + \mathbf{g}(t, \omega), \quad (11)$$

where  $\mathbf{A}_f(\omega_d)$  is the  $3 \times 3$  Jacobian matrix evaluated at  $\omega_d$ , i.e.,

$$\mathbf{A}_f(\omega_d) = \left. \frac{\partial \mathbf{f}}{\partial \omega} \right|_{\omega_d} = \begin{bmatrix} \frac{\partial f_1}{\partial \omega_1} & \frac{\partial f_1}{\partial \omega_2} & \frac{\partial f_1}{\partial \omega_3} \\ \frac{\partial f_2}{\partial \omega_1} & \frac{\partial f_2}{\partial \omega_2} & \frac{\partial f_2}{\partial \omega_3} \\ \frac{\partial f_3}{\partial \omega_1} & \frac{\partial f_3}{\partial \omega_2} & \frac{\partial f_3}{\partial \omega_3} \end{bmatrix} \Bigg|_{\omega_d}, \quad (12)$$

and  $\mathbf{g}(t, \omega)$  is the nonlinear residual in the linearization of  $\mathbf{f}(\omega)$ , which also satisfies

$$\mathbf{g}(t, \omega) = \mathbf{f}(\omega) - \mathbf{f}(\omega_d) - \mathbf{A}_f(\omega_d)(\omega - \omega_d). \quad (13)$$

The explicit dependence of  $\mathbf{g}$  on  $t$  reflects the fact that  $\omega_d$  is a reference function that explicitly depends on time, as discussed in [1].

Now, subtracting (10) from (8) yields

$$J\dot{e}_\omega + \mathbf{A}_f(\omega_d)e_\omega + \mathbf{g}(t, \omega) = \tau - \tau_d. \quad (14)$$

Concurrently, by defining  $\mathbf{v} = \left[ \frac{\lambda^2}{s+\lambda} K_I \right] e_\omega$ , we rewrite the control law in (7) as

$$\tau - \tau_d = -(\mathbf{K}_P + \lambda \mathbf{K}_I) e_\omega + \mathbf{v}, \quad (15)$$

which allows us to restate (14) as

$$\dot{e}_\omega = -J^{-1}(\mathbf{A}_f(\omega_d) + \mathbf{K}_P + \lambda \mathbf{K}_I) e_\omega + J^{-1}\mathbf{v} - J^{-1}\mathbf{g}(t, \omega), \quad (16)$$

$$\dot{\mathbf{v}} = \lambda^2 \mathbf{K}_I e_\omega - \lambda \mathbf{v}. \quad (17)$$

Then, noticing that  $\mathbf{g}$  depends directly on  $e_\omega$  only, as

$$\mathbf{g}(t, \omega) = \mathbf{g}(e_\omega) = \begin{bmatrix} (j_{33} - j_{22})e_{\omega_2}e_{\omega_3} \\ (j_{11} - j_{33})e_{\omega_1}e_{\omega_3} \\ (j_{22} - j_{11})e_{\omega_1}e_{\omega_2} \end{bmatrix}, \quad (18)$$

it follows that (16) and (17) can be written in the state-space

form

$$\dot{\boldsymbol{x}} = \boldsymbol{\eta}(t, \boldsymbol{x}), \quad (19)$$

where  $\boldsymbol{\eta} : [0, \infty) \times \mathbb{R}^6 \rightarrow \mathbb{R}^6$  is defined as

$$\boldsymbol{\eta}(t, \boldsymbol{x}) = \begin{bmatrix} -\boldsymbol{J}^{-1}(\boldsymbol{A}_f(\boldsymbol{\omega}_d) + \boldsymbol{K}_p + \lambda \boldsymbol{K}_1) & \boldsymbol{J}^{-1} \\ \lambda^2 \boldsymbol{K}_1 & -\lambda \boldsymbol{I}_3 \end{bmatrix} \boldsymbol{x} + \begin{bmatrix} -\boldsymbol{J}^{-1} \boldsymbol{g}(\boldsymbol{e}_\omega) \\ \mathbf{0}_{3 \times 1} \end{bmatrix}, \quad (20)$$

with the system's state  $\boldsymbol{x}(t) = [\boldsymbol{e}_\omega^T(t) \ \boldsymbol{v}^T(t)]^T$ .

Thus, the problem of controller synthesis and stability analysis becomes a standard problem of stability *motion*, where it is desirable for the system's output  $\boldsymbol{\omega}$  to remain close to the reference motion trajectory  $\boldsymbol{\omega}_d$ . The stability of the state-space representation of the system in (19) can be analyzed by employing Lyapunov's direct method for nonautonomous systems [2], [3], provided that a number of required properties are satisfied. In particular, it can be shown that  $\boldsymbol{\eta}(t, \boldsymbol{x})$  is continuous as long as the desired trajectory  $\boldsymbol{\omega}_d$  is smooth and physically feasible. Also, it can be shown that (19) has a unique equilibrium point at the origin and satisfies the local Lipschitz condition required for the use of Theorem 4.10 in [3]. The proofs of these last two claims are presented in parts A and B of the Appendix.

To employ Lyapunov's direct method, we first define a *proto*-Lyapunov function that depends explicitly on the controller parameters  $\boldsymbol{K}_p = \text{diag}\{k_{p1}, k_{p2}, k_{p3}\}$  and  $\boldsymbol{K}_1 = \text{diag}\{k_{11}, k_{12}, k_{13}\}$ . Here, we choose a function with the form

$$\begin{aligned} \mu(\boldsymbol{x}) &= \frac{1}{2} \boldsymbol{x}^T \begin{bmatrix} \boldsymbol{J} & \mathbf{0}_{3 \times 3} \\ \mathbf{0}_{3 \times 3} & \frac{1}{\lambda^2} \boldsymbol{K}_1^{-1} \end{bmatrix} \boldsymbol{x} \\ &= \frac{1}{2} \boldsymbol{e}_\omega^T \boldsymbol{J} \boldsymbol{e}_\omega + \frac{1}{2\lambda^2} \boldsymbol{v}^T \boldsymbol{K}_1^{-1} \boldsymbol{v}, \end{aligned} \quad (21)$$

which, for a set  $\mathcal{K}_K = \{k_{p1}, k_{p2}, k_{p3}, k_{11}, k_{12}, k_{13}\}$  of stabilizing parameters, becomes a Lyapunov stability function for the state-space representation in (19). Note that  $\mu(\mathbf{0}) = 0$  and

$$\mu(\boldsymbol{x}) > 0, \quad \forall \boldsymbol{x} \neq \mathbf{0}, \quad (22)$$

provided that  $\boldsymbol{K}_1$  is chosen to be positive definite by design, because  $\boldsymbol{J}$  is always positive definite. Furthermore, it follows directly from (21) that

$$\begin{aligned} \min \left\{ \frac{1}{2} \lambda_{\min} \{\boldsymbol{J}\}, \frac{1}{2\lambda^2} \lambda_{\min} \{\boldsymbol{K}_1^{-1}\} \right\} (|\boldsymbol{e}_\omega|_2^2 + |\boldsymbol{v}|_2^2) \\ \leq \mu(\boldsymbol{x}) \leq \\ \max \left\{ \frac{1}{2} \lambda_{\max} \{\boldsymbol{J}\}, \frac{1}{2\lambda^2} \lambda_{\max} \{\boldsymbol{K}_1^{-1}\} \right\} (|\boldsymbol{e}_\omega|_2^2 + |\boldsymbol{v}|_2^2), \end{aligned} \quad (23)$$

where the operators  $\lambda_{\min}\{\cdot\}$  and  $\lambda_{\max}\{\cdot\}$  extract the smallest and largest eigenvalues of a square matrix, respectively. Also, note that

$$\dot{\mu}(\boldsymbol{x}) = \boldsymbol{e}_\omega^T \boldsymbol{J} \dot{\boldsymbol{e}}_\omega + \frac{1}{\lambda^2} \boldsymbol{v}^T \boldsymbol{K}_1^{-1} \dot{\boldsymbol{v}}, \quad (24)$$

which evaluated along the system's trajectory, becomes

$$\begin{aligned} \dot{\mu}(\boldsymbol{x}) &= -\boldsymbol{e}_\omega^T (\boldsymbol{K}_p + \lambda \boldsymbol{K}_1) \boldsymbol{e}_\omega - \boldsymbol{e}_\omega^T \boldsymbol{A}_f(\boldsymbol{\omega}_d) \boldsymbol{e}_\omega \\ &\quad - \boldsymbol{e}_\omega^T \boldsymbol{g}(\boldsymbol{e}_\omega) + 2\boldsymbol{e}_\omega^T \boldsymbol{v} - \frac{1}{\lambda} \boldsymbol{v}^T \boldsymbol{K}_1^{-1} \boldsymbol{v}. \end{aligned} \quad (25)$$

Further analysis shows that  $\dot{\mu}(\boldsymbol{x})$  in (25) is negative definite provided that  $\lambda$ ,  $\boldsymbol{K}_p$ ,  $\boldsymbol{K}_1$  and  $\boldsymbol{\omega}_d$  satisfy certain conditions. This is the key element in the method for controller synthesis presented in this paper.

To continue, note that

$$\boldsymbol{e}_\omega^T \boldsymbol{A}_f(\boldsymbol{\omega}_d) \boldsymbol{e}_\omega = \boldsymbol{e}_\omega^T \tilde{\boldsymbol{A}}_f(\boldsymbol{\omega}_d) \boldsymbol{e}_\omega, \quad (26)$$

where  $\tilde{\boldsymbol{A}}_f(\boldsymbol{\omega}_d)$  is a symmetric matrix computed as

$$\tilde{\boldsymbol{A}}_f(\boldsymbol{\omega}_d) = \frac{1}{2} \left( \boldsymbol{A}_f(\boldsymbol{\omega}_d) + \boldsymbol{A}_f^T(\boldsymbol{\omega}_d) \right). \quad (27)$$

Since for any signal  $\boldsymbol{\omega}_d$  the matrix  $\tilde{\boldsymbol{A}}_f(\boldsymbol{\omega}_d)$  is Hermitian, for any time  $t$ , all its eigenvalues are real. Also, from simple algebraic manipulations, given that the axes of  $\mathcal{B}$  are aligned with the principal axes of inertia of the flyer, it can be shown that the control error  $\boldsymbol{e}_\omega$  is orthogonal to the nonlinear residual  $\boldsymbol{g}(\boldsymbol{e}_\omega)$ , i.e.,

$$\boldsymbol{e}_\omega^T \boldsymbol{g}(\boldsymbol{e}_\omega) = 0. \quad (28)$$

Thus, (26) and (28) allow us to simplify (25) to obtain

$$\begin{aligned} \dot{\mu}(\boldsymbol{x}) &= -\boldsymbol{e}_\omega^T (\boldsymbol{K}_p + \lambda \boldsymbol{K}_1) \boldsymbol{e}_\omega - \boldsymbol{e}_\omega^T \tilde{\boldsymbol{A}}_f(\boldsymbol{\omega}_d) \boldsymbol{e}_\omega \\ &\quad + 2\boldsymbol{e}_\omega^T \boldsymbol{v} - \frac{1}{\lambda} \boldsymbol{v}^T \boldsymbol{K}_1^{-1} \boldsymbol{v}, \end{aligned} \quad (29)$$

which establishes that there exist feasible sets of controller parameters,  $\mathcal{K}_K$ , and functions  $\boldsymbol{\omega}_d$ ,  $\mathcal{K}_{\boldsymbol{\omega}_d}$ , for which the function  $\dot{\mu}(\boldsymbol{x})$  becomes negative definite. This fact can be deduced from noticing that

$$-\boldsymbol{e}_\omega^T \boldsymbol{A}_f(\boldsymbol{\omega}_d) \boldsymbol{e}_\omega \leq -\lambda_{\min} \left\{ \tilde{\boldsymbol{A}}_f(\boldsymbol{\omega}_d) \right\} |\boldsymbol{e}_\omega|_2^2 \quad (30)$$

$$= -\tilde{d}(t) |\boldsymbol{e}_\omega|_2^2 \leq -\underline{d} |\boldsymbol{e}_\omega|_2^2,$$

$$-\boldsymbol{e}_\omega^T \boldsymbol{K}_p \boldsymbol{e}_\omega \leq -\lambda_{\min} \{ \boldsymbol{K}_p \} |\boldsymbol{e}_\omega|_2^2 = -k_p |\boldsymbol{e}_\omega|_2^2, \quad (31)$$

$$-\boldsymbol{e}_\omega^T \boldsymbol{K}_1 \boldsymbol{e}_\omega \leq -\lambda_{\min} \{ \boldsymbol{K}_1 \} |\boldsymbol{e}_\omega|_2^2 = -k_1 |\boldsymbol{e}_\omega|_2^2, \quad (32)$$

$$-\boldsymbol{v}^T \boldsymbol{K}_1^{-1} \boldsymbol{v} \leq -\lambda_{\min} \{ \boldsymbol{K}_1^{-1} \} |\boldsymbol{v}|_2^2 = -\frac{1}{k_1} |\boldsymbol{v}|_2^2, \quad (33)$$

where the eigenvalue  $\tilde{d}$  is a function of time, because  $\boldsymbol{\omega}_d$  is a function of time, lower-bounded by  $\underline{d} = \min_t \{ \tilde{d}(t) \}$ . Since  $\boldsymbol{K}_p$  and  $\boldsymbol{K}_1$  are designed to be constant, diagonal and positive definite, the eigenvalues  $k_p$ ,  $k_1$  and  $1/k_1$  are positive constant numbers.

Then, by directly applying (30)–(33), we can bound  $\dot{\mu}(\boldsymbol{x})$  as

$$\dot{\mu}(\boldsymbol{x}) \leq -(\underline{d} + \lambda k_1 + k_p) |\boldsymbol{e}_\omega|_2^2 + 2\boldsymbol{e}_\omega^T \boldsymbol{v} - \frac{1}{\lambda k_1} |\boldsymbol{v}|_2^2, \quad (34)$$

from which we can derive a recipe for controller synthesis and a Lyapunov-based method for stability analysis. These objectives are accomplished by defining a real number  $\beta > 0$  and noticing that

$$\begin{aligned} &-(\underline{d} + \lambda k_1 + k_p) |\boldsymbol{e}_\omega|_2^2 + 2\boldsymbol{e}_\omega^T \boldsymbol{v} - \frac{1}{\lambda k_1} |\boldsymbol{v}|_2^2 \\ &= -\left( \underline{d} + \lambda k_1 + k_p - \frac{1}{\beta} \right) |\boldsymbol{e}_\omega|_2^2 - \left( \frac{1}{\lambda k_1} - \beta \right) |\boldsymbol{v}|_2^2 \\ &\quad - \left| \frac{1}{\sqrt{\beta}} \boldsymbol{e}_\omega - \sqrt{\beta} \boldsymbol{v} \right|_2^2, \end{aligned} \quad (35)$$

from which it follows that the strict negativity of  $\dot{\mu}(\boldsymbol{x})$  ( $\dot{\mu}(\boldsymbol{x}) < 0, \forall \boldsymbol{x} \neq \mathbf{0}$ ) is enforced by satisfying

$$0 < \frac{1}{\underline{d} + \lambda k_1 + k_p} < \beta < \frac{1}{\lambda k_1}. \quad (36)$$

Furthermore, if (36) is enforced, we also have that

$$\dot{\mu}(\boldsymbol{x}) \leq -\min \left\{ \underline{d} + k_1 \lambda + k_p - \frac{1}{\beta}, \frac{1}{k_1 \lambda} - \beta \right\} |\boldsymbol{x}|_2^2. \quad (37)$$

Thus far, we have shown that for a diagonal positive definite matrix  $\boldsymbol{K}_1$ , the function  $\mu(\boldsymbol{x})$  is positive definite,

and that for parameters satisfying (36), the function  $\dot{\mu}(\mathbf{x})$  is strictly negative along any feasible trajectory  $\omega_d$ . Additionally, we showed that  $\mu(\mathbf{x})$  is bounded by two simple state-dependent quadratic expressions, and that  $\dot{\mu}(\mathbf{x})$  is upper-bounded by a simple state-dependent quadratic expression. These facts are crucial in proving the exponential stability of the nonautonomous system described by (19). Formally, we state the main result of this work as a series of mathematical claims, proven using standard techniques.

*Claim 1:* By properly choosing a reference trajectory  $\omega_d$ , the nonautonomous system  $\dot{\mathbf{x}} = \boldsymbol{\eta}(t, \mathbf{x})$ , defined by (19) and (20), is forced to have a unique fixed point  $\mathbf{x}^* = \mathbf{0}$ .

*Proof:* See Part A of the Appendix. ■

*Claim 2:* By properly choosing a reference trajectory  $\omega_d$ , the function  $\boldsymbol{\eta}(t, \mathbf{x}) : [0, \infty) \times \mathbb{R}^6 \rightarrow \mathbb{R}^6$  is forced to be continuous in  $t$  and locally Lipschitz in  $\mathbf{x}$  on  $[0, \infty) \times \mathbb{D}_x$ , where  $\mathbb{D}_x = \{\mathbf{x} : \|\mathbf{e}_\omega\|_2 \leq r_{e_\omega} \in \mathbb{R}^+; \mathbf{v} \in \mathbb{R}^3\}$ .

*Proof:* See Part B of the Appendix. ■

*Claim 3:* The only fixed point of the closed-loop nonautonomous system  $\dot{\mathbf{x}} = \boldsymbol{\eta}(t, \mathbf{x})$ ,  $\mathbf{x}^* = \mathbf{0}$ , is locally exponentially stable on  $\mathbb{D}_x$ , provided that the inequalities in (36) are satisfied, i.e.,  $0 < 1/(\underline{d} + \lambda k_1 + k_p) < \beta < 1/(\lambda \bar{k}_1)$ .

*Proof:* Acknowledging Claim 1, Claim 2, (23) and (37), the proof immediately follows from the direct application of Theorem 4.10 on Page 154 of [3]. ■

Now, after defining

$$\gamma_1 = \min \left\{ \frac{1}{2} \lambda_{\min} \{ \mathbf{J} \}, \frac{1}{2\lambda^2} \lambda_{\min} \{ \mathbf{K}_I^{-1} \} \right\}, \quad (38)$$

$$\gamma_2 = \max \left\{ \frac{1}{2} \lambda_{\max} \{ \mathbf{J} \}, \frac{1}{2\lambda^2} \lambda_{\max} \{ \mathbf{K}_I^{-1} \} \right\}, \quad (39)$$

$$\gamma_3 = \min \left\{ \underline{d} + k_1 \lambda + k_p - \frac{1}{\beta}, \frac{1}{\bar{k}_1 \lambda} - \beta \right\}, \quad (40)$$

directly from Claim 3, we can also conclude that

$$\dot{\mu} \leq -\gamma_3 \|\mathbf{x}\|_2^2 \leq -\frac{\gamma_3}{\gamma_2} \mu, \quad (41)$$

from which, applying basic linear theory, it follows that

$$\mu(t) \leq e^{-\frac{\gamma_3}{\gamma_2}(t-t_0)} \mu(t_0), \quad (42)$$

and consequently, that

$$\|\mathbf{x}(t)\|_2 \leq \sqrt{\frac{\gamma_2}{\gamma_1}} e^{-\frac{\gamma_3}{2\gamma_2}(t-t_0)} \|\mathbf{x}(t_0)\|_2. \quad (43)$$

Therefore, we can conclude that for any finite initial condition  $\mathbf{x}(t_0)$ , in the absence of disturbances, the control error along the desired trajectory  $\omega_d$ ,  $\mathbf{e}_\omega$ , will decay to zero at the rate  $\gamma_3/2\gamma_2$ . Both  $\gamma_3/2\gamma_2$  and  $\sqrt{\gamma_2/\gamma_1}$  depend directly on the controller parameters  $\{\lambda, \mathbf{K}_p, \mathbf{K}_I\}$  and  $\omega_d$ . Clearly, the closed-loop system's performance increases by making  $\gamma_3/2\gamma_2$  large and  $\sqrt{\gamma_2/\gamma_1}$  small. However, the selection of  $\{\gamma_1, \gamma_2, \gamma_3\}$  is constrained by the stability condition in (36) and physical limitations of the flyer's actuators.

From an analytical perspective, (36) provides us with a tool for analyzing the system's stability, given predefined controller parameters  $\lambda$ ,  $\mathbf{K}_p$  and  $\mathbf{K}_I$ , and a reference  $\omega_d$ . Any controller-reference combination satisfying  $0 < 1/(\underline{d} + \lambda k_1 + k_p) < 1/(\lambda \bar{k}_1)$  defines an exponentially stable closed-loop system. From a design perspective, (36) provides us with a tool for controller synthesis. One can start by choosing any  $0 < \beta \in \mathbb{R}^+$ , then any quadruplet  $\{\lambda, \mathbf{K}_p, \mathbf{K}_I, \omega_d\}$  with parameters satisfying (36) define a stable closed-loop

nonautonomous system represented as in (19). Theoretically, employing this analysis, the problem of controller synthesis can be formulated as a multi-objective optimization problem, which is matter of current and further research. In this work, the controller parameters are tuned experimentally and  $\omega_d$  is chosen so that it defines a desired high-speed multi-flip maneuver while satisfying the feasible region determined by (36).

Note that the proof of Claim 3 establishes that the only fixed point of the closed-loop nonautonomous system described by (19),  $\mathbf{x}^* = \mathbf{0}$ , is locally exponentially stable and not necessarily globally exponentially stable, because the proof is based on Claim 2, which establishes that the function  $\boldsymbol{\eta}(t, \mathbf{x})$  is only locally Lipschitz. However, we can prove that the equilibrium point  $\mathbf{x}^* = \mathbf{0}$  is globally exponentially stable using other arguments. From Appendix B, it follows that  $\boldsymbol{\eta}(t, \mathbf{x})$  is locally Lipschitz in  $\mathbf{x}$  on the domain  $\mathbb{D}_x = \{\mathbf{x} : \|\mathbf{e}_\omega\|_2 \leq r_{e_\omega} \in \mathbb{R}^+; \mathbf{v} \in \mathbb{R}^3\}$ . Then, assuming that the initial condition  $\|\mathbf{x}(t_0)\|_2$  is finite,  $\mathbb{D}_x$  is defined to satisfy  $r_{e_\omega} \geq \sqrt{\gamma_2/\gamma_1} \|\mathbf{x}(t_0)\|_2$ , which means that  $\mathbf{x}^* = \mathbf{0}$  is exponentially stable as long as the initial condition  $\|\mathbf{x}(t_0)\|_2$  is finite.

## B. Attitude and Translational Dynamics

Thus far, we have shown that by choosing the right controller parameters, the angular velocity  $\omega$  will converge to a physically feasible  $\omega_d$  at an exponential rate. The next challenge is to understand how the quadrotor's attitude evolves during the execution of a controlled multi-flip maneuver. First, we note that the attitude state dynamics described by (4) can be thought of as an open-loop system with input  $\omega$  and output  $\mathbf{q}$ , as depicted in Fig. 2. Then, we show that for signals  $\omega$  and  $\mathbf{q}$  generated according to the control structure in Fig. 2, the error between the *true* body frame  $\mathcal{B}$  and the *ideal* reference flipping frame  $\mathcal{I}$  remains bounded during a multi-flip maneuver. This is equivalent to saying that the attitude error remains bounded. This analytical fact is further supported by experimental results.

In the proposed scheme shown in Fig. 2, in the absence of sensor noise, the *true* measured angular velocity of the flyer is  $\omega$ . As explained before,  $\omega$  is defined with respect to the inertial frame  $\mathcal{N}$  with its components expressed in  $\mathcal{B}$ . Thus, recalling that  $\mathbf{q}$  denotes the *true* attitude of  $\mathcal{B}$ , it follows that

$$\dot{\mathbf{q}} = \frac{1}{2} \mathbf{q} * \mathbf{p}, \quad \text{with } \mathbf{p} = \begin{bmatrix} 0 & \omega^T \end{bmatrix}^T. \quad (44)$$

Consistently with the control scheme in Fig. 2, the desired angular velocity  $\omega_d$  is defined with respect to  $\mathcal{N}$  with its components expressed in  $\mathcal{B}$ . However, the dynamics of the desired attitude  $\mathbf{q}_d$  cannot be straightforwardly related to  $\omega_d$  the way  $\mathbf{q}$  is related to  $\omega$  in (44) because due to the absence of attitude feedback control, the space orientations of  $\mathcal{I}$  and  $\mathcal{B}$  over time might differ with respect to each other. Instead, the dynamics of  $\mathbf{q}_d$  are determined by

$$\dot{\mathbf{q}}_d = \frac{1}{2} \mathbf{q}_d * \hat{\mathbf{p}}_d, \quad \text{with } \hat{\mathbf{p}}_d = \begin{bmatrix} 0 & \hat{\omega}_d^T \end{bmatrix}^T, \quad (45)$$

where  $\hat{\omega}_d$  has exactly the same components as  $\omega_d$ , but is expressed in  $\mathcal{I}$  rather than  $\mathcal{B}$ .

Thus, from the previous definitions, it follows that the attitude quaternion error between  $\mathbf{q}_d$  and  $\mathbf{q}$  is

$$\mathbf{q}_e = \mathbf{q}_d^{-1} * \mathbf{q}, \quad (46)$$

as discussed in [23]. Then, differentiating with respect to time yields

$$\dot{\mathbf{q}}_e = -\mathbf{q}_d^{-1} * \dot{\mathbf{q}}_d * \mathbf{q}_d^{-1} * \mathbf{q} + \mathbf{q}_d^{-1} * \dot{\mathbf{q}}, \quad (47)$$

which using (44) and (45) can be rewritten as

$$\dot{\mathbf{q}}_e = \frac{1}{2} \mathbf{q}_e * (\mathbf{p} - \mathbf{q}^{-1} * \mathbf{q}_d * \hat{\mathbf{p}}_d * \mathbf{q}_d^{-1} * \mathbf{q}) = \frac{1}{2} \mathbf{q}_e * \mathbf{p}_e, \quad (48)$$

where  $\mathbf{p}_e$  is an expression for the angular velocity error between  $\hat{\omega}_d$  and  $\omega$ . This result follows from expressing  $\hat{\mathbf{p}}_d$  in  $\mathcal{B}$ , then calculating the difference with respect to  $\mathbf{p}$  in  $\mathcal{B}$ .

Since the ideal reference flipping axis is invariant in both  $\mathcal{N}$  and  $\mathcal{I}$ , we know that  $\mathbf{q}_d * \hat{\mathbf{p}}_d * \mathbf{q}_d^{-1} = \hat{\mathbf{p}}_d$ . The attitude error quaternion  $\mathbf{q}_e$  contains the information about the rotation axis and the rotation angle between  $\mathcal{I}$  and  $\mathcal{B}$ . In this work, we measure the attitude error by computing the rotation angle corresponding to the scalar part of  $\mathbf{q}_e = [m_e \ \mathbf{n}_e^T]^T$ , employing the methods and identities in [22]. Thus, after some algebraic manipulations and recalling that  $\mathbf{q}$  is a unit quaternion, i.e.,  $q_0^2 + q_1^2 + q_2^2 + q_3^2 = 1$ , we obtain

$$\begin{aligned} \dot{m}_e &= \frac{1}{2} (d_2 q_3 - d_3 q_2) (\omega_1 + \nu_1) + \frac{1}{2} (d_3 q_1 - d_1 q_3) (\omega_2 + \nu_2) \\ &+ \frac{1}{2} (d_1 q_2 - d_2 q_1) (\omega_3 + \nu_3) + \frac{1}{2} (d_1 q_0 - d_0 q_1) (\omega_1 - \nu_1) \\ &+ \frac{1}{2} (d_2 q_0 - d_0 q_2) (\omega_2 - \nu_2) + \frac{1}{2} (d_3 q_0 - d_0 q_3) (\omega_3 - \nu_3), \end{aligned} \quad (49)$$

where  $\mathbf{q}_d = [d_0 \ d_1 \ d_2 \ d_3]^T$  and  $\hat{\mathbf{p}}_d = [0 \ \nu_1 \ \nu_2 \ \nu_3]^T$ . Also, as explained in [1], the ideal reference flipping axis is described by a unit vector  $\mathbf{a}_f = [a_1 \ a_2 \ a_3]^T$  expressed in  $\mathcal{I}$ . Thus, for an ideal reference angle  $\Psi$ ,  $\hat{\omega}_d = \Psi \mathbf{a}_f$ , it follows that

$$\begin{bmatrix} d_0 \\ d_1 \\ d_2 \\ d_3 \end{bmatrix} = \begin{bmatrix} \cos \frac{\Psi}{2} \\ a_1 \sin \frac{\Psi}{2} \\ a_2 \sin \frac{\Psi}{2} \\ a_3 \sin \frac{\Psi}{2} \end{bmatrix}, \quad \begin{bmatrix} \nu_1 \\ \nu_2 \\ \nu_3 \end{bmatrix} = \begin{bmatrix} a_1 \Psi \\ a_2 \Psi \\ a_3 \Psi \end{bmatrix}. \quad (50)$$

Then, noticing that  $d_3 \nu_2 - d_2 \nu_3 = d_1 \nu_3 - d_3 \nu_1 = d_2 \nu_1 - d_1 \nu_2 = 0$ , we can write

$$\begin{aligned} \dot{m}_e &= \frac{1}{2} (d_2 q_3 - d_3 q_2 + d_1 q_0 - d_0 q_1) (\omega_1 - \nu_1) \\ &+ \frac{1}{2} (d_3 q_1 - d_1 q_3 + d_2 q_0 - d_0 q_2) (\omega_2 - \nu_2) \\ &+ \frac{1}{2} (d_1 q_2 - d_2 q_1 + d_3 q_0 - d_0 q_3) (\omega_3 - \nu_3). \end{aligned} \quad (51)$$

Now, recalling from the previous section that the components of  $\omega$ ,  $\{\omega_1, \omega_2, \omega_3\}$ , will entry-wise converge to  $\{\nu_1, \nu_2, \nu_3\}$  at an exponential rate, we can conclude that  $\dot{m}_e$  will converge to zero and  $m_e$  will approach a constant value. Furthermore, since the angle that measures the attitude error is given by  $\Theta = 2 \arccos m_e$ , we can also conclude that the error between  $\mathcal{B}$  and  $\mathcal{I}$  will remain bounded during a high-speed multi-flip maneuver. In fact, it can be shown that

$$\Theta(t) \leq \frac{2\gamma_2 \sqrt{\gamma_2}}{\gamma_3 \sqrt{\gamma_1}} \left(1 - e^{-\frac{\gamma_3}{2\gamma_2}(t-t_0)}\right) |e_\omega(t_0)|_2 + \Theta(t_0). \quad (52)$$

This analytical result is consistent with the experimental results discussed in the next section of this paper.

During a multi-flip maneuver, in the absence of powerful disturbances, the translational motion of the quadrotor undergoes an ascent-descent process in which gravity is the

only significant non-actuated exerted force on the system. Since the execution of a multi-flip maneuver normally takes less than 2 s, the drift of the quadrotor on the inertial  $n_1$ - $n_2$  plane is small relative to the size of the flyer. This statement is consistent with the experimental results discussed in the next section of the paper. However, note that the open-loop translational dynamics are unstable.

#### IV. SIMULATIONS AND EXPERIMENTAL RESULTS

In this section, we present simulations and experimental results that validate the proposed Lyapunov-based method for controller synthesis and analysis. The flyer's parameters and physical variables involved in numerical computation and control implementation are expressed in the *meter-kilogram-second* (MKS) system of units. As examples, we consider three high-speed reference trajectories  $\omega_d$ , corresponding to single-, double- and triple-flip maneuvers about the body axis  $\mathbf{b}_1$ , where the associated eigenvalues  $\underline{d}$  are  $-4.5326 \times 10^{-5}$  N·m·s/rad,  $-5.1801 \times 10^{-5}$  N·m·s/rad and  $-5.8277 \times 10^{-5}$  N·m·s/rad, respectively. In all the cases,  $\mathbf{K}_P = k_P \mathbf{I}_3$ ,  $\mathbf{K}_I = k_I \mathbf{I}_3$ , and the controller parameters are chosen to be  $\lambda = 30$  rad/s,  $k_P = 2 \times 10^{-3}$  N·m·s/rad and  $k_I = 6 \times 10^{-5}$  N·m·s<sup>2</sup>/rad. Also, it can be verified that  $\beta = 555.5536$  rad/N·m·s satisfies the inequalities in (36), and therefore, the only equilibrium point  $\mathbf{x}^* = \mathbf{0}$  of the closed-loop system defined by (19) and (20) is ensured to be nominally exponentially stable, provided that the initial condition  $|\mathbf{x}(t_0)|_2$  is finite.

Simulation results of the three considered cases are shown in Figs. 3-(a), 3-(b) and 3-(c). The reference flipping speed,  $|\omega_d(t)|_2$ , is shown in *green*, the simulated controlled flipping speed,  $\omega_1(t)$ , is shown in *blue* and the simulated flipping angle about  $\mathbf{b}_1$  (roll) is shown in *red*. The almost-perfect matching between the green and blue curves demonstrates the achievement of both high performance and stability under nominal conditions. Experimental results of the three considered cases are shown in Figs. 3-(d), 3-(e) and 3-(f). The reference flipping speed,  $|\omega_d(t)|_2$ , is shown in *green*, the measured controlled flipping speed,  $\omega_1(t)$ , is shown in *blue* and the measured flipping angle about  $\mathbf{b}_1$  (roll) is shown in *red*. These results demonstrate that the proposed control scheme enables the robust execution of real-time high-speed multi-flip maneuvers, from both the stability and performance perspectives, even in the presence of plant uncertainty and disturbances. Here, plant uncertainty comes mostly from unmodeled aerodynamic effects and variability of the actuator parameters. Disturbances come from the changing atmospheric conditions surrounding the flyer.

In the course of this research, the proposed control scheme has been tested through several dozens of real-time flight experiments. Six of these flight experiments are shown in Fig. 4. Here, Figs. 4-(a), 4-(b) and 4-(c) show composite images of single-, double- and triple-flip maneuvers about the  $\mathbf{b}_1$  axis, respectively. Similarly, Figs. 4-(d), 4-(e) and 4-(f) show composite images of single-, double- and triple-flip maneuvers about a 45°-oblique axis,  $\mathbf{b}'_1 = (\mathbf{b}_1 + \mathbf{b}_2)/\sqrt{2}$ , respectively. Complete videos of these six experiments can be found in [24].

#### V. CONCLUSIONS

We proposed a Lyapunov-based method for synthesizing and analyzing controllers capable of automatically flying a

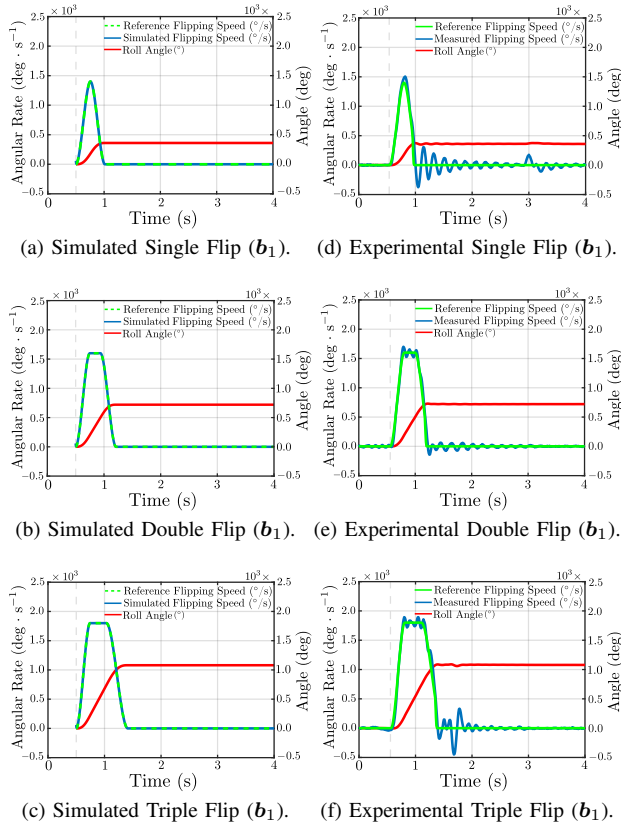


Fig. 3: **Simulations and experimental results.** Plots (a), (b) & (c) show simulations of single-, double- and triple-flip high-speed maneuvers about the body-fixed axis  $\mathbf{b}_1$ . The simulations start at  $t_0 = 0.5$  s. Plots (d), (e) & (f) show real-time experiments of single-, double- and triple-flip high-speed maneuvers about the body-fixed axis  $\mathbf{b}_1$ . The experiments start at  $t_0 = 0.5$  s.

19-gram quadrotor during high-speed multi-flip maneuvers. The method for controller design is based on the use of an angular velocity feedback structure and a parameterized *proto*-Lyapunov function associated with the closed-loop system. We showed analytically that, in the absence of plant uncertainty and disturbances, the flyer’s angular velocity converges to a multi-flip reference signal, provided that this reference is physically feasible and smooth. In this case, from the feasible set of controller parameters, we experimentally selected gains that made the system robust from both the stability and performance perspectives. In addition, using quaternion representation, we showed that during a high-speed multi-flip maneuver, the proposed controller causes the attitude error to remain bounded. Simulation and experimental flight results clearly demonstrate the suitability of the proposed approach.

#### REFERENCES

- [1] Y. Chen and N. O. Pérez-Arancibia, “Generation and Real-Time Implementation of High-Speed Controlled Maneuvers Using an Autonomous 19-Gram Quadrotor,” in *Proc. 2016 IEEE Int. Conf. Robot. Autom. (ICRA 2016)*, Stockholm, Sweden, May 2016, pp. 3204–3211.
- [2] J.-J. E. Slotine and W. Li, *Applied Nonlinear Control*. Upper Saddle River, NJ: Prentice-Hall, Inc., 1991.
- [3] K. K. Hassan, *Nonlinear Systems, 3rd*. Upper Saddle River, NJ: Prentice-Hall, Inc., 2002.
- [4] S. Schaal, “Dynamic Movement Primitives -A Framework for Motor Control in Humans and Humanoid Robotics,” in *Adaptive Motion of Animals and Machines*, H. Kimura, K. Tsuchiya, A. Ishiguro, and H. Witte, Eds. Tokyo: Springer, 2006, ch. 6, pp. 261–280.

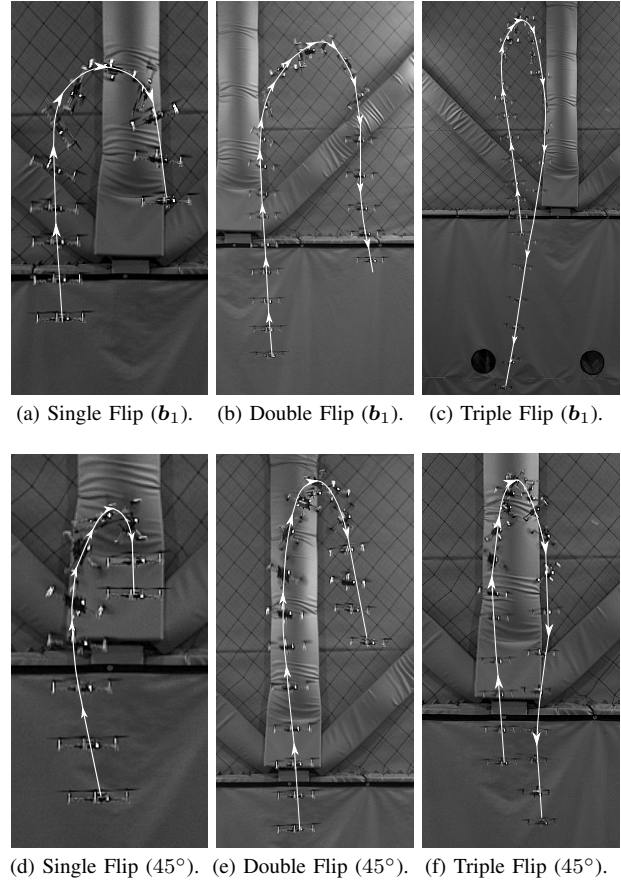


Fig. 4: **Real-time flight experiments.** Composite images of six high-speed maneuvers. Trajectories (a), (b) & (c) correspond to single-, double- and triple-flip maneuvers about the body-fixed axis  $\mathbf{b}_1$ . Trajectories (d), (e) & (f) correspond to single-, double- and triple-flip maneuvers about the  $45^\circ$ -oblique axis  $\mathbf{b}'_1 = (\mathbf{b}_1 + \mathbf{b}_2)/\sqrt{2}$ . The complete movie with all the cases is available at <http://www.uscaml.com/resources/MultiFlipACC.mp4>.

- [5] R. M. Murray, D. C. Deno, K. S. J. Pister, and S. S. Sastry, “Control Primitives for Robot Systems,” *IEEE Trans. Syst., Man, Cybern.*, vol. 22, no. 1, pp. 183–193, Jan./Feb. 1992.
- [6] N. O. Pérez-Arancibia, P.-E. J. Duhamel, K. Y. Ma, and R. J. Wood, “Model-Free Control of a Flapping-Wing Microrobot,” in *Proc. 16th Int. Conf. Adv. Robot. (ICAR 2013)*, Montevideo, Uruguay, Nov. 2013, pp. 1–8.
- [7] —, “Model-Free Control of a Hovering Flapping-Wing Microrobot,” *J. Intell. Robot. Syst.*, vol. 77, no. 1, pp. 95–111, Jan. 2015.
- [8] A. Das, F. Lewis, and K. Subbarao, “Backstepping Approach for Controlling a Quadrotor Using Lagrange Form Dynamics,” *J. Intell. Robot. Syst.*, vol. 56, no. 1–2, pp. 127–151, Sep. 2009.
- [9] T. Madani and A. Benallegue, “Backstepping Control for a Quadrotor Helicopter,” in *Proc. 2006 IEEE/RSJ Int. Conf. Intell. Robots Syst. (IROS 2006)*, Beijing, China, Oct. 2006, pp. 3255–3260.
- [10] —, “Control of a Quadrotor Mini-Helicopter via Full State Backstepping Technique,” in *Proc. 45th IEEE Conf. Decis. Control (CDC 2006)*, San Diego, CA, Dec. 2006, pp. 1515–1520.
- [11] D. Lee, H. J. Kim, and S. Sastry, “Feedback Linearization vs. Adaptive Sliding Mode Control for a Quadrotor Helicopter,” *Int. J. Control Autom. Syst.*, vol. 7, no. 3, pp. 419–428, Jun. 2009.
- [12] H. Bouadi, S. S. Cunha, A. Drouin, and F. Mora-Camino, “Adaptive Sliding Mode Control for Quadrotor Attitude Stabilization and Altitude Tracking,” in *IEEE 12th Int. Symp. Comput. Intell. Informat.*, Budapest, Hungary, Nov. 2011, pp. 449–455.
- [13] C. Coza and C. J. B. Macnab, “A New Robust Adaptive-Fuzzy Control Method Applied to Quadrotor Helicopter Stabilization,” in *North. Amer. Fuzzy. Inf. Process. Soc.*, Canada, Jun. 2006, pp. 454–458.
- [14] A. Tayebi and S. McGilvray, “Attitude Stabilization of a VTOL Quadrotor Aircraft,” *IEEE Trans. Control Syst. Technol.*, vol. 14, no. 3, pp. 562–571, May. 2006.
- [15] S. Bouabdallah, P. Murrieri, and R. Siegwart, “Design and Control of

An Indoor Micro Quadrotor," in *Proc. 2004 IEEE Int. Conf. Robot. Autom.*, vol. 5, New Orleans, USA, Apr. 2004, pp. 4393–4398.

- [16] A. Das, K. Subbarao, and F. Lewis, "Dynamic Inversion with Zero-Dynamics Stabilisation for Quadrotor Control," *IET Control. Theory. Appl.*, vol. 3, no. 3, pp. 303–314, Mar. 2009.
- [17] T. Lee, M. Leoky, and N. H. McClamroch, "Geometric Tracking Control of A Quadrotor UAV on SE (3)," in *Proc. 2010 IEEE Conf. Decis. Control (CDC 2010)*, Atlanta, USA, Dec. 2010, pp. 5420–5425.
- [18] T. Dierks and S. Jagannathan, "Output Feedback Control of A Quadrotor UAV Using Neural Networks," *IEEE Trans. Neural Netw.*, vol. 21, no. 1, pp. 50–66, Jan. 2010.
- [19] D. Mellinger, N. Michael, and V. Kumar, "Trajectory Generation and Control for Precise Aggressive Maneuvers with Quadrotors," *Int. J. Robot. Res.*, vol. 31, no. 5, pp. 664–674, Apr. 2012.
- [20] S. Lupashin, A. Schöllig, M. Sherback, and R. D'Andrea, "A Simple Learning Strategy for High-Speed Quadcopter Multi-Flips," in *Proc. 2010 IEEE Int. Conf. Robot. Autom. (ICRA 2010)*, Anchorage, USA, May. 2010, pp. 1642–1648.
- [21] <https://wiki.bitcraze.io/projects:crazyflie:index>.
- [22] J. B. Kuipers, *Quaternions and Rotation Sequences*. Princeton, NJ: Princeton University Press, 1999, vol. 66.
- [23] R. Mahony, T. Hamel, and J.-M. Pfimlin, "Nonlinear Complementary Filters on the Special Orthogonal Group," *IEEE Trans. Autom. Control*, vol. 53, no. 5, pp. 1203–1218, Jun. 2008.
- [24] <http://www.uscaml.com/resources/MultiFlipACC.mp4>.

## APPENDIX

### A. The Only Fixed Point of the Closed-Loop System is $\mathbf{0}$

In the proposed control structure of Fig. 2, the closed-loop system defined by (19) is forced to have a unique fixed point at  $\mathbf{x}^* = \mathbf{0}$ , where  $\mathbf{x}^* = [e_\omega^{*T} \ v^{*T}]^T$ , by properly choosing a reference trajectory  $\omega_d$ . To begin the argument, notice that for a fixed point  $\mathbf{x}^*$  it follows that  $\eta(t, \mathbf{x}^*) = \mathbf{0}$  for all  $t \geq 0$ , which implies that

$$\mathbf{0} = -(\mathbf{K}_P + \lambda \mathbf{K}_I + \mathbf{A}_f(\omega_d)) e_\omega^* + v^* - g(e_\omega^*), \quad (53)$$

$$\mathbf{0} = -\lambda v^* + \lambda^2 \mathbf{K}_I e_\omega^*. \quad (54)$$

Then, by combining both equations above we obtain

$$(\mathbf{K}_P + \mathbf{A}_f(\omega_d)) e_\omega^* + g(e_\omega^*) = \mathbf{0}. \quad (55)$$

Clearly, if  $e_\omega^* = \mathbf{0}$ , then from (54) it follows that  $v^* = \mathbf{0}$  and  $\mathbf{x}^* = \mathbf{0}$ . By definition of fixed point,  $e_\omega^*$  is constant, so follows that  $g(e_\omega^*)$  is also constant.

Now, we show that there exists a set of physically feasible reference trajectories  $\omega_d$  for which  $\mathbf{x}^* = \mathbf{0}$  is the unique fixed point of the closed-loop system defined by (19) and (20). Specifically, the previous statement is true for all references of the form

$$\omega_d = \varpi \mathbf{a}, \quad (56)$$

where  $\varpi$  is a nonnegative bell-shaped function, as defined in [1], and  $\mathbf{a}$  is a unit vector that describes the corresponding flipping axis, expressed in the body frame  $\mathcal{B}$ . Formally, for a reference defined as in (56), the relationship (55) is satisfied if and only if  $e_\omega^* = \mathbf{0}$ . The proof of necessity ( $\Leftarrow$  direction) immediately follows from noticing that if  $e_\omega^* = \mathbf{0}$ , then  $g(e_\omega^*) = \mathbf{0}$ . The proof of sufficiency ( $\Rightarrow$  direction) can be established employing the *contradiction technique* and noticing that, for all  $\omega_d$  of the form given in (56), (55) cannot be satisfied by a nonzero constant  $e_\omega^*$  for all time  $t \geq 0$ . A time-varying  $e_\omega^*$  contradicts the definition of fixed point, which completes the argument.

Note that an  $\omega_d$  can easily be constructed so that (55) is satisfied by multiple nonzero constant values of  $e_\omega^*$  for all

$t \geq 0$ . Also note that it is not trivial to determine the set of all the references  $\omega_d$  that force the closed-loop system to have a unique fixed point at  $\mathbf{0}$ .

### B. The Function $\eta(t, \mathbf{x})$ is Continuous and Locally Lipschitz

Here, we show that by properly choosing the reference  $\omega_d$ ,  $\eta(t, \mathbf{x})$  is ensured to be continuous and locally Lipschitz. To begin, we rewrite the nonautonomous system as

$$\dot{\mathbf{x}} = \eta(t, \mathbf{x}) = \mathbf{F}(t)\mathbf{x} + \zeta(\mathbf{x}), \quad (57)$$

where

$$\mathbf{F}(t) = \begin{bmatrix} -\mathbf{J}^{-1}(\mathbf{A}_f(\omega_d) + \mathbf{K}_P + \mathbf{K}_I\lambda) & \mathbf{J}^{-1} \\ \lambda^2 \mathbf{K}_I & -\lambda \mathbf{I}_3 \end{bmatrix}, \quad (58)$$

$$\zeta(\mathbf{x}) = \begin{bmatrix} -\mathbf{J}^{-1}g(e_\omega) \\ \mathbf{0}_{3 \times 1} \end{bmatrix}. \quad (59)$$

In  $\mathbf{F}(t)$ ,  $\mathbf{A}_f(\omega_d)$  is a function of  $\omega_d$ , which depends on a nonnegative bell-shaped function  $\varpi$ , as defined in (56). Since  $\varpi$  is a polynomial function of  $t$  without discontinuities or singularities, it immediately follows that  $\eta(t, \mathbf{x})$  is continuous in  $t \geq 0$ .

Now, we show that  $\eta(t, \mathbf{x})$  is locally Lipschitz in  $\mathbf{x}$ . We begin by considering two feasible states  $\mathbf{x}$  and  $\mathbf{y}$  to obtain

$$|\eta(t, \mathbf{x}) - \eta(t, \mathbf{y})|_2 \leq \|\mathbf{F}(t)\|_2 |\mathbf{x} - \mathbf{y}|_2 + |\zeta(\mathbf{x}) - \zeta(\mathbf{y})|_2, \quad (60)$$

where the induced 2-norm  $\|\mathbf{F}(t)\|_2$  can be chosen to remain bounded by a proper selection of the reference  $\omega_d(t)$ . The remaining step is to find a Lipschitz constant for  $|\zeta(\mathbf{x}) - \zeta(\mathbf{y})|_2$ . To accomplish this objective, we first obtain the  $6 \times 6$  Jacobian matrix

$$\frac{\partial \zeta}{\partial \mathbf{x}} = \left[ \begin{array}{ccc|cc} 0 & -\frac{\alpha_{32}}{j_{11}} e_{\omega_3} & -\frac{\alpha_{32}}{j_{11}} e_{\omega_2} & & \\ -\frac{\alpha_{13}}{j_{22}} e_{\omega_3} & 0 & -\frac{\alpha_{13}}{j_{22}} e_{\omega_1} & & \\ -\frac{\alpha_{21}}{j_{33}} e_{\omega_2} & -\frac{\alpha_{21}}{j_{33}} e_{\omega_1} & 0 & & \\ \hline & \mathbf{0}_{3 \times 3} & & \mathbf{0}_{3 \times 3} & \end{array} \right], \quad (61)$$

where  $\alpha_{32} = j_{33} - j_{22}$ ,  $\alpha_{13} = j_{11} - j_{33}$  and  $\alpha_{21} = j_{22} - j_{11}$ . Then, considering that on the domain  $\mathbb{D}_x = \{\mathbf{x} : |e_\omega|_2 \leq r_{e_\omega} \in \mathbb{R}^+; \mathbf{v} \in \mathbb{R}^3\}$ , both  $\zeta(\mathbf{x})$  and  $\partial \zeta / \partial \mathbf{x}$  are forced to be continuous in  $t$ , we use Lemmas 3.1 and 3.2 from [3]. To continue, note that the induced  $\infty$ -norm of the matrix  $\partial \zeta / \partial \mathbf{x}$  is bounded on  $\mathbb{D}_x$  according to the inequality

$$\left\| \frac{\partial \zeta}{\partial \mathbf{x}} \right\|_\infty \leq \sqrt{3} \max \left\{ \left| \frac{\alpha_{32}}{j_{11}} \right|, \left| \frac{\alpha_{13}}{j_{22}} \right|, \left| \frac{\alpha_{21}}{j_{33}} \right| \right\} r_{e_\omega} = L_\zeta. \quad (62)$$

Thus, it follows that

$$\left\| \frac{\partial \zeta}{\partial \mathbf{x}} \right\|_2 \leq \sqrt{3} \left\| \frac{\partial \zeta}{\partial \mathbf{x}} \right\|_\infty \leq \sqrt{3} L_\zeta, \quad (63)$$

which implies that  $\zeta(\mathbf{x})$  is locally Lipschitz on  $\mathbb{D}_x$  and that  $\sqrt{3} L_\zeta$  is a Lipschitz constant for  $\zeta(\mathbf{x})$ . Consequently, it also follows that

$$|\eta(t, \mathbf{x}) - \eta(t, \mathbf{y})|_2 \leq L_\eta |\mathbf{x} - \mathbf{y}|_2, \quad (64)$$

where  $L_\eta = \max_{t \geq t_0} \|\mathbf{F}(t)\|_2 + \sqrt{3} L_\zeta$ . We can thus conclude that  $\eta(t, \mathbf{x})$  is locally Lipschitz on  $\mathbb{D}_x$  and that  $L_\eta$  is a Lipschitz constant for  $\eta(t, \mathbf{x})$ .